SCIENTIFIC REPORTS
nature research

OPEN

Novel electronic properties of monoclinic MP_4 (M = Cr, Mo, W) compounds with or without topological nodal line

Muhammad Rizwan Khan[1,2], Kun Bu[1,2], Jun-Shuai Chai[1,2] & Jian-Tao Wang[1,2,3]✉

Transition metal phosphides hold novel metallic, semimetallic, and semiconducting behaviors. Here we report by *ab initio* calculations a systematical study on the structural and electronic properties of MP_4 (M = Cr, Mo, W) phosphides in monoclinic *C2/c* (C_{2h}^6) symmetry. Their dynamical stabilities have been confirmed by phonon modes calculations. Detailed analysis of the electronic band structures and density of states reveal that CrP_4 is a semiconductor with an indirect band gap of 0.47 eV in association with the *p* orbital of P atoms, while MoP_4 is a Dirac semimetal with an isolated nodal point at the Γ point and WP_4 is a topological nodal line semimetal with a closed nodal ring inside the first Brillouin zone relative to the *d* orbital of Mo and W atoms, respectively. Comparison of the phosphides with group VB, VIB and VIIB transition metals shows a trend of change from metallic to semiconducting behavior from VB-MP_4 to VIIB-MP_4 compounds. These results provide a systematical understandings on the distinct electronic properties of these compounds.

Transition metal phosphides (TMPs) have been attracted considerable research interest due to their structural and compositional diversity that results in a broad range of novel electronic, magnetic and catalytic properties[1–4]. This family consists of large number of materials, having distinct crystallographic structures and morphologies because of choices of different TMs and phosphorus atoms[5]. These compounds have been studied extensively due to their outstanding physical and chemical properties such as high catalytic activity[6], good electrical conductivity[7], and magnetocaloric behaviors[8,9]. TMPs have been appeared as an efficient catalyst for hydrogen evolution reduction (HER)[4,10–13]. For example, nanowires of FeP and FeP_2 have been used widely for hydrogen evolution in both strong alkaline and acidic aqueous solutions[10]. CoP[11], CoP_3[12], and MoP_2[13] are also reported as an excellent materials for HER and oxygen evolution reduction (OER) due to their good stability. Moreover, phosphorus rich phases have been found more effective for HER and OER, and have better stability because of the presence of a large number of negatively charge P-atom centers[14,15]. In addition to electrocatalysis process, TMPs have various potential device applications, such as usage in electrotonic components, luminescent and semiconductor devices and as an anode material in lithium-ion batteries[16–19]. Moreover, some TMPs such as TaP[20] hold topological Weyl semimetal feature, and WP has been recently reported to have Dirac like points near the Fermi level[21]. Similarly, transition metal diphosphide compounds, like MoP_2 and WP_2, were predicated as type-II Weyl topological semimetals[22].

Topological semimetals are not only of fundamental physical interests but also of great potential for future applications in quantum computation and spintronics[23–28]. In topological semimetals, topological non-trivial band crossing points or line (line of nodes) exist in three-dimensional (3D) Brillouin zone (BZ) protected by certain symmetries[29,30]. It can be classified into Dirac semimetal[31], Weyl semimetal[32,33] and nodal line semimetal (NLSM)[30,34–37]. Driac semimetals have been theoretically predicted and experimentally confirmed in several materials such as Cd_3As_2[31] and Na_3Bi[37]. Topological Weyl semimetals have paring two-fold degenerate Weyl

[1]Beijing National Laboratory for Condensed Matter Physics, Institute of Physics, Chinese Academy of Sciences, Beijing 100190, China. [2]School of Physical Sciences, University of Chinese Academy of Sciences, Beijing 100049, China. [3]Songshan Lake Materials Laboratory, Dongguan 523808, Guangdong, China. ✉email: wjt@aphy.iphy.ac.cn

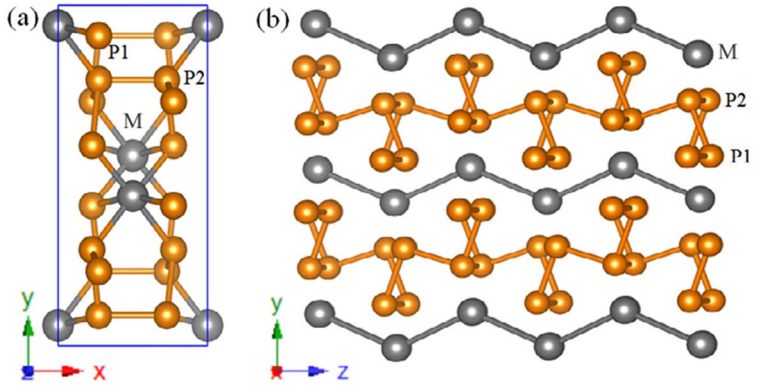

Figure 1. Crystal structure of MP_4 (M = Cr, Mo, W) compounds. (**a**) The unit cell in monoclinic *C*2/*c* symmetry. (**b**) the layered view. The M atoms are depicted in black while the P atoms are depicted in orange. These structures were drawn using VESTA package[76].

Compound	Atom	Position	*x*	*y*	*z*
CrP_4	Cr	4*e*	0.0000	0.9398	0.2500
	P_1	8*f*	0.2280	0.4105	0.8238
	P_2	8*f*	0.2731	0.7815	0.1919
MoP_4	Mo	4*e*	0.0000	0.9409	0.2500
	P_1	8*f*	0.2211	0.4055	0.8168
	P_2	8*f*	0.2774	0.7779	0.1893
WP_4	W	4*e*	0.0000	0.9406	0.2500
	P_1	8*f*	0.2219	0.4056	0.8173
	P_2	8*f*	0.2768	0.7780	0.1884

Table 1. Atomic coordinates and Wyckoff positions for MP_4 (M = Cr, Mo, W) compounds in monoclinic *C*2/*c* symmetry.

points with opposite distinct chiralities that may be right handed or left handed and have been realized in the materials breaking the time reversal (*T*) symmetry such as pyrochlore iridate[33] or spatial inversion (*P*) symmetry such as TaAs family of compounds[38]. In NLSMs, the bands crossing points form continuous line rather than discrete points, generally enforced due to the band inversion mechanism[39,40] and protected by *PT* symmetry[34]. Topological NLSMs have been found in CaP_3[41], Ca_3P_2[42] phosphides and 3D graphene network structures[43–54], etc.

In this paper, based on ab initio calculations, we systematically investigate the transition metal phosphides MP_4 (M = Cr, Mo, W) for the structural stability and electronic properties. These three compounds are all in monoclinic phase with *C*2/*c* (C^6_{2h}) symmetry, while CrP_4 and MoP_4 have been experimentally synthesized[55] and WP_4 is not yet reported. Their mechanical stabilities are confirmed with phonon mode analysis. Electronic band calculations show that CrP_4 is a semiconductor with an indirect band gap of 0.47 eV, MoP_4 is a topological Dirac semimetal with isolated band crossing at the Γ point, and WP_4 is a topological nodal line semimetal with a closed nodal ring inside the first BZ. We also make a comparison of the phosphides with group VB and VIIB transition metals and a trend of change from metallic to semiconducting is observed from VB-MP_4 to VIIB-MP_4 compounds.

Results and discussion

We first present the structural characterization. Figure 1a shows the structure of monoclinic compounds of MP_4 (M = Cr, Mo, W) in *C*2/*c* (C^6_{2h}, No. 15) symmetry. The M atoms are depicted in black occupying the 4*e* Wyckoff positions, while there are two kinds of P atoms (P_1 and P_2) depicted in orange occupying two distinct 8*f* Wyckoff positions, respectively, as listed in Table 1. The metals environments in MP_4 compounds can be described as the octahedral coordination environment, in which metal atoms are always octahedrally surrounded by P atoms, while P atoms have tetrahedrally coordinated environment. Basically, the crystalline structure of monoclinic MP_4 compounds can be seen as a layered structure of black phosphorus in which metal atoms are inserted[56] between two buckled phosphorus layers (Fig. 1b). Metal atoms intercalate and reorder the atomic stacks similar to Na atom insertion in black phosphorus[57]. A sandwiched structure is formed where wave like metal atom layers are in between the two buckled phosphorus layers.

There are three unique types of bonds in monoclinic compounds MP_4, namely M-P_1, M-P_2, and P_1-P_2 chemical bonds. In CrP_4, the bond lengths are 2.277–2.373 Å for Cr-P_1, 2.316 Å for Cr-P_2, and 2.215–2.240 Å for P_1-P_2; in MoP_4, the bond lengths are 2.396–2.456 Å for Mo-P_1, 2.456 Å for Mo-P_2, and 2.208–2.243 Å for P_1-P_2; while in WP_4, the bond lengths are 2.398–2.477 Å for W-P_1, 2.453 Å for W-P_2, and 2.215–2.245 Å for P_1-P_2. Meanwhile,

Compound	Method	a(Å)	b(Å)	c(Å)	β(°)	$d_{(M-P1)}$(Å)	$d_{(M-P2)}$(Å)	$d_{(P-P)}$(Å)	∠P-M-P(°)	E_g (eV)
CrP_4	PBE	5.196	10.754	5.717	110.42	2.277–2.373	2.316	2.215–2.240	85.30–92.37	0.47
	Exp[55]	5.191	10.760	5.771	110.65					
	PBE[58]	5.170	10.684	5.692	110.03					0.63
MoP_4	PBE	5.337	11.207	5.855	110.72	2.396–2.456	2.456	2.208–2.243	83.80–94.0	Semimetal
	Exp[55]	5.313	11.139	5.820	110.64					
	PBE[59]	5.268	11.090	5.798	110.80					
WP_4	PBE	5.344	11.195	5.876	110.95	2.398–2.475	2.453	2.215–2.245	84.16–93.83	Semimetal

Table 2. Calculated equilibrium lattice parameters (a, b, c and β), bond lengths (d_{M-P1}, d_{M-P2}, and d_{P-P}), and electronic band gap E_g for MP_4 (M = Cr, Mo, W) compounds, comparing with experimental and previously calculated data[55,58,59].

there are three distinct types of bond angles depicted as $\angle P_1$-M-P_1, $\angle P_2$-M-P_2 and $\angle P_1$-M-P_2. For CrP_4, the bond angles are 90.03° for $\angle P_1$-Cr-P_1, 85.30° for $\angle P_2$-Cr-P_2, and 92.37° for $\angle P_1$-Cr-P_2; for MoP_4, the bond angles are 88.19° for $\angle P_1$-Mo-P_1, 83.80° for $\angle P_2$-Mo-P_2, and 94.0° for $\angle P_1$-Mo-P_2; while for WP_4, the bond angles are 88.19° for $\angle P_1$-W-P_1, 84.16° for $\angle P_2$-W-P_2, and 93.83° for $\angle P_1$-W-P_2. It can be seen that the bond lengths between P-P atoms are almost same in the three MP_4 compounds, while the bond lengths between Mo-P and W-P atoms are clearly larger than that between Cr-P atoms. Meanwhile, $\angle P_1$-M-P_2 are found larger than the other angles in all MP_4 compounds. The calculated equilibrium lattice parameters, bond lengths, and bond angles for MP_4 compounds are listed in Table 2. It is seen that our calculated structural parameters matches well with the reported experimental and calculated data[55,58,59].

To examine the dynamical stability of MP_4 compounds, we have calculated the phonon band structures and partial phonon density of states (PDOS) with equilibrium lattice parameters in a $2 \times 2 \times 2$ supercell, as shown in Fig. 2. For CrP_4, MoP_4 and WP_4, no imaginary frequencies occur in the whole BZ and PDOS, thus confirming the structural stability of the three compounds. There are some similarities in the phonon band structures and PDOS for CrP_4, MoP_4 and WP_4 due to the same space symmetry groups and elementary components for the three compounds. The highest vibrational frequencies all happen near the Γ point and the values are 519.8 cm^{-1} for CrP_4, 521.8 cm^{-1} for MoP_4 and 526.8 cm^{-1} for WP_4, respectively. It is seen from the PDOS that the lower frequency modes are mainly contributed by the metal atoms because of their heavier masses while the higher frequency modes are mainly contributed by the P atoms with lighter masses.

Next we discuss the electronic properties of MP_4 (M = Cr, Mo, W) compounds. Figure 3 represents the calculated electronic band structures along the high symmetry directions of the BZ using HSE06 functional[60] and the fermi energy (E_F) is set to zero. For CrP_4 as shown in Fig. 3a, the conduction band minimum (CBM) is located along H-Z direction and valence band maximum (VBM) is located along F-H direction, showing a semiconducting behavior with an indirect band gap of 0.47 eV, which is smaller than the reported direct band gap of 0.63 eV[58]. For MoP_4 as shown in Fig. 3b, the lowest conduction band and highest valence band are degenerate at Γ point near the E_F, indicating that MoP_4 is a Dirac semimetal with a four-fold degenerate Dirac point at the Γ point[61]. Moreover, our calculations show that the valence and conduction bands of WP_4 exhibit linear dispersion near the E_F and cross along the Γ-X high symmetry direction (Fig. 3c) due to the band inversion mechanism[39,40]. To further explore the topological electronic properties, we establish a tight binding (TB) model using the maximally localized Wannier functions (MLWFs)[62,63] to search the nodal points in the 3D BZ. We find that the nodal points (or band crossing points) of valence and conduction bands in WP_4 form a continuous nodal ring in the full BZ (see Fig. 3d), thus, WP_4 can be termed as a topological nodal line semimetal with a closed nodal ring protected by PT symmetry[34,35,41].

It is interesting to notice that although Cr, Mo and W are all in the VIB group of the Periodic Table of Elements, CrP_4 is an indirect band gap semiconductor, MoP_4 is a Dirac semimetal with a single nodal point, and WP_4 is a nodal line semimetal with a closed nodal ring. The metallicity of CrP_4, MoP_4, and WP_4 grows with the increase of the elementary ordinal from **3d** to **5d** transition metals. To further understand the electronic properties, we have plotted the total and partial density of states (DOS) of MP_4 compounds as shown in Fig. 4. For CrP_4 (Fig. 4a), there is a band gap of 0.47 eV as depicted in Fig. 3a. The states around the Fermi level are mainly contributed by the p states of P atoms (Fig. 4b), relative to the covalent bonds between P-P atoms. For MoP_4 (Fig. 4c), there is a little peak on the Fermi level, the states at the Fermi level are mainly composed of d orbital of Mo atoms (see Fig. 4d). Moreover, for WP_4 (Fig. 4e), there is a little peak on the Fermi level, but larger than that in MoP_4, the states at the Fermi level are predominantly composed of P-p orbital and W-d orbital (Fig. 4f). It can be inferred that the electronic behaviors in CrP_4 are mainly dominated by the P-P covalent bonds in CrP_4, so that CrP_4 tend to be a semiconductor due to covalent bonding properties between P-P atoms. While in MoP_4 and WP_4, the electronic properties are largely determined by the metal atoms which have metallic bonds with P atoms, so that they show semimetallic properties. The small peaks on the Fermi level in MoP_4 and WP_4 semimetals are related to the band touching point between the top of valance and the bottom of conduction bands. Similar DOSs around the Fermi level are also found in CaP_3 family of nodal line semimetals[41].

We have further examined the band structures of MoP_4 and WP_4 with spin-orbital coupling (SOC) as shown in Fig. S1 in Supplementary Information. For MoP_4, the SOC induced band gap is about 0.1 meV at the Γ point, while for WP_4, the SOC induced band gap is about 29 meV along the high-symmetric X-Γ direction. We can

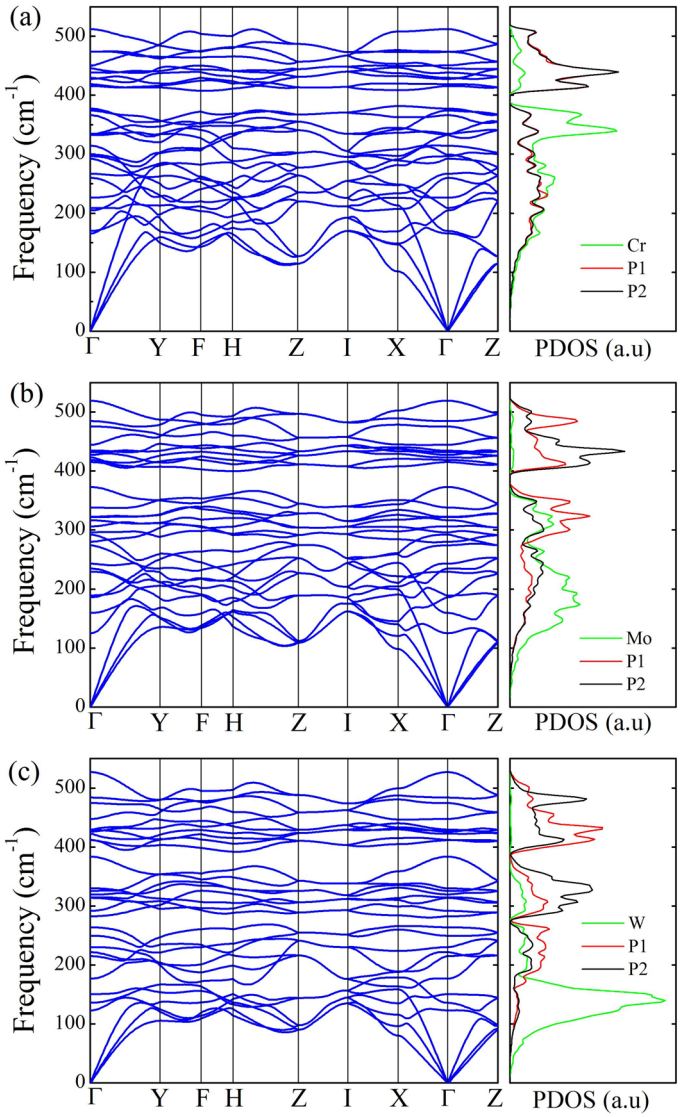

Figure 2. Phonon band structures and density of states (PDOS) for MP_4 (M = Cr, Mo, W) compounds at equilibrium lattice parameters. The lower frequency modes are mainly contributed by the metal atoms because of their heavier masses while the higher frequency modes are mainly contributed by the P atoms with lighter masses.

see that when SOC is included, MoP_4 and WP_4 become strong topological insulators with the symmetry-based indicators[64–66] (z_2, z_2, z_2, z_4) as (0,0,0,1), like as the finding in CaP_3 family of materials[41].

In order to better understand the electronic properties of VIB-MP_4 (M = Cr, Mo, W) compounds, we have also examined the electronic properties of the VP_4, NbP_4, TaP_4, MnP_4, TcP_4 and ReP_4, while V, Nb and Ta are in the VB group, and Mn, Tc and Re are in the VIIB group, which are all next to Cr, Mo and W in the Periodic Table of Elements. The TcP_4 and ReP_4 are experimentally synthesized by the reaction of their constituent elements[67–69]. The calculated equilibrium lattice parameters and electronic band structures are given in Table S1 and Fig. S2 in Supplementary Information, respectively. The structural parameters and electronic behavior that is, VP_4 is metallic and MnP_4 is a semiconductor reported by Gong et al.[58]. We find that VB-MP_4 (M = V, Nb, Ta) have metallic behavior, while VIIB-MP_4 (M = Mn, Tc, Re) are semiconductors. It is clearly seen that from VB-MP_4 to VIIB-MP_4, the metallicity of these phosphides grow weaker with a change from metallic to semiconducting, while from top (**3d**) to bottom (**5d**) in each group, the metallicity of these phosphides grow stronger. So it is reasonable that CrP_4 should be a semiconductor, MoP_4 is a semimetal with isolated nodal points and WP_4 is a topological nodal line semimetal with a line of nodes.

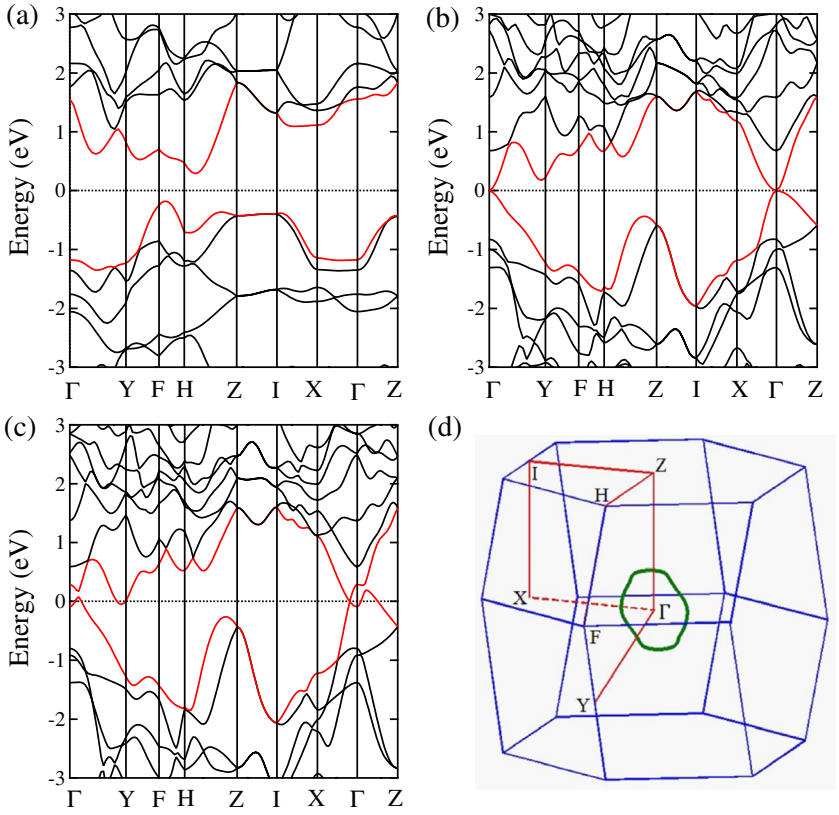

Figure 3. Electronic band structures for (**a**) CrP_4, (**b**) MoP_4 and (**c**) WP_4 at equilibrium lattice parameters using HSE06 functional (without spin-orbital coupling). (**d**) The BZ with several high-symmetry points indicated at Γ (0.00, 0.00, 0.00), Y (0.3067, 0.3067, 0.0440), F (0.3631, 0.3631, 0.3937), H (0.2503, 0.2503, 0.6943), Z (0.00, 0.00, 0.50), I (0.50, −0.50, 0.50), and X (0.50, −0.50, 0.00). The nodal ring (green circle) in (**d**) is formed by band crossing points for WP_4 compound were plotted using MATLAB software.

Conclusions

In conclusion, we have performed a systematic ab initio study on MP_4 (M = Cr, Mo, W) monoclinic compounds. Their dynamical stabilities have been confirmed by phonon modes calculations. Electron band structures calculations show that CrP_4 is an indirect band gap semiconductor with a narrow band gap of 0.47 eV, MoP_4 is Dirac semimetal and WP_4 is considered as a new candidate for topological nodal line semimetal with a closed nodal ring in the first BZ protected by the *PT* symmetry. The electronic density of states calculations indicate that in CrP_4, the valence and conduction bands near the Fermi level are mainly contributed by the *p* orbitals of P atoms, while in MoP_4 and WP_4, there is a little peak on the Fermi level and the energy bands are mainly composed of *d* orbitals of Mo and W atoms, respectively. We also make a comparison of the phosphides with group VB and VIIB transition metals and a trend of change from metallic to semiconducting is observed from VB-MP_4 to VIIB-MP_4 compounds. These results provide a systematic understanding and pave the way for further experimental explorations on the transition metal phosphides.

Methods

Our calculations were carried out using the density functional theory as implemented in the Vienna ab initio simulation package (VASP)[70]. The projector augmented wave (PAW)[71] method was adopted with valence electrons of $3s^2 3p^3$ for P, $3p^6 3d^5 4s^1$ for Cr, $4p^6 4d^5 5s^1$ for Mo, and $5p^6 5d^4 6s^1$ for W. Generalized gradient approximation (GGA) developed by Perdew, Burke and Ernzerhof (PBE)[72] is used as the exchange-correlation potential. A $5 \times 8 \times 6$ Monkhorst-Pack grid of BZ sampling is used and an energy cutoff of 500 eV is set for the plane-wave basis. The structures are fully optimized until the total energy difference is less then 10^{-6} eV and convergence criteria for atomic forces is set to be 10^{-3} eV/Å. The electronic properties are calculated with the Heyd–Scuseria–Ernzerhof hybrid functional (HSE06)[60] and the phonon properties are calculated with phononpy package[73]. To further explore the topological electronic properties, we establish a tight binding (TB) model using the maximally localized Wannier functions (MLWFs)[62,63] implemented in Wannier90 package[74] and searched the band crossing points in the entire BZ with WannierTools pacakge[75].

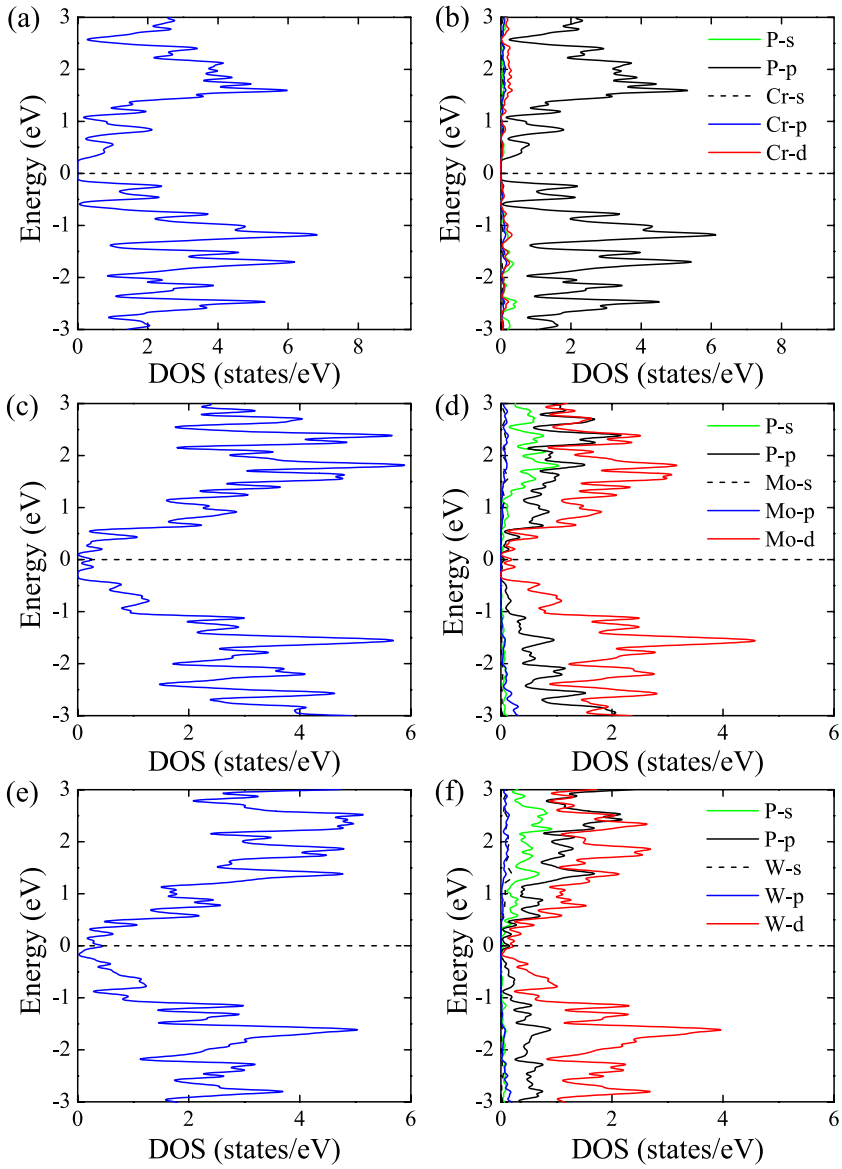

Figure 4. Total and partial density of states (DOS) for MP_4 (M = Cr, Mo, W) compounds at equilibrium lattice parameters using HSE06 functional (without spin-orbital coupling). (**a, b**) Total and partial DOSs for CrP_4; (**c, d**) Total and partial DOSs for MoP_4; and (**e, f**) Total and partial DOSs for WP_4.

Received: 27 March 2020; Accepted: 1 June 2020
Published online: 13 July 2020

References

1. Whitmire, K. H. & Caudell, J. B. First row transition metal phosphides, in encyclopedia of inorganic and bioinorganic chemistry. *John Wiley Sons Ltd***1–8**, https://doi.org/10.1002/9781119951438.eibc2160 (2013).
2. Chen, W. F., Muckerman, J. T. & Fujita, E. Recent developments in transition metal carbides and nitrides as hydrogen evolution electrocatalysts. *Chem. Commun.***49**, 8896–8909. https://doi.org/10.1039/C3CC44076A (2013).
3. Veillard, A. Ab initio calculations of transition-metal organometallics: structure and molecular properties. *Chem. Rev.***91**, 743–766. https://doi.org/10.1021/cr00005a006 (1991).
4. Feng, L. & Huaiguo, X. advances of transition metal phosphide application in electrochemical energy storage and catalysis. *ChemElectroChem.***4**, 20–34. https://doi.org/10.1002/celc.201600563 (2017).
5. Jing, H. C. & Kenton, H. W. A structural survey of the binary transition metal phosphides and arsenides of the d-block elements. *Coord. Chem. Rev.***355**, 271–327. https://doi.org/10.1016/j.ccr.2017.08.029 (2018).
6. Du, H., Gu, S., Liu, R. & Li, C. M. Highly active and inexpensive iron phosphide nanorods electrocatalyst towards hydrogen evolution reaction. *Int. J. Hydrog Energy***40**, 14272–14278. https://doi.org/10.1016/j.ijhydene.2015.02.099 (2015).
7. Carenco, S., Portehault, D., Boissiere, C., Mezailles, N. & Sanchez, C. Nanoscaled metal borides and phosphides: recent developments and perspectives. *Chem. Rev.***113**, 7981–8065. https://doi.org/10.1021/cr400020d (2013).
8. Yang, S., Liang, C. & Prins, R. Preparation and hydrotreating activity of unsupported nickel phosphide with high surface area. *J. Catal.***241**, 465–469. https://doi.org/10.1016/j.jcat.2006.05.014 (2006).

9. Muetterties, E. L. & Sauer, J. C. Catalytic properties of metal phosphides: I. Qualitative assay of catalytic properties. *J. Am. Chem. Soc.***96**, 3410–3415. https://doi.org/10.1021/ja00818a012 (1974).
10. Son, C. Y., Kwak, I. H., Lim, Y. R. & Park, J. FeP and FeP_2 nanowires for efficient electrocatalytic hydrogen evolution reaction. *Chem. Commun.***52**, 2819–2822. https://doi.org/10.1039/C5CC09832G (2016).
11. Liu, M. & Li, J. Cobalt phosphide hollow polyhedron as efficient bifunctional electrocatalysts for the evolution reaction of hydrogen and oxygen. *J. ACS. Appl. Mater. Interfaces***8**, 2158–2165. https://doi.org/10.1039/C3CC44076A (2016).
12. Wu, T., Pi, M., Wang, X., Zhang, D. & Chen, S. Three-dimensional metalrganic framework derived porous CoP_3 concave polyhedrons as superior bifunctional electrocatalysts for the evolution of hydrogen and oxygen. *Phys. Chem. Chem. Phys.***19**, 2104–2110. https://doi.org/10.1039/C3CC44076A (2017).
13. Pu, Z., Amiinu, I. S., Wang, M., Yang, Y. & Mu, S. Semimetallic MoP_2: an active and stable hydrogen evolution electrocatalyst over the whole pH range. *Nanoscale***8**, 8500–8504. https://doi.org/10.1039/C3CC44076A (2016).
14. Xiao, P. *et al.* Molybdenum phosphide as an efficient electrocatalyst for the hydrogen evolution reaction. *Energy Environ. Sci.***8**, 2624–2629. https://doi.org/10.1039/C3CC44076A (2015).
15. Shi, Y. & Zhang, B. Recent advances in transition metal phosphide nanomaterials: synthesis and applications in hydrogen evolution reaction. *Chem. Soc. Rev.***6**, 1529–1541. https://doi.org/10.1039/C5CS00434A (2016).
16. Dmitruk, N. L., Zuev, V. A. & Stepanova, M. A. Spectral distribution of the photoconductivity of cadmium diphosphide. *Russ. Phys. J.***34**, 642–644. https://doi.org/10.1039/C3CC44076A (1991).
17. Lazarev, V. B., Shevchenko, V. Y., Grinberg, L. K. & Sobolev. V. V. Semiconducting II-V Compounds. *Nauka Moscow, Russia,* (1976).
18. Morozova, V. A., Marenkin, S. F., Koshelev, O. G. & Trukhan, V. M. Optical absorption in monoclinic zinc diphosphide. *Inorg. Mater.***42**, 221–225. https://doi.org/10.1039/C3CC44076A (2006).
19. Oyama, S. T., Gott, T., Zhao, H. & Lee, Y. K. Transition metal phosphide hydroprocessing catalysts: a review. *Catal. Today***143**, 94–107. https://doi.org/10.1039/C3CC44076A (2009).
20. Xu, N. *et al.* Observation of Weyl nodes and Fermi arcs in tantalum phosphide. *Nat. Commun.***7**, 11006–11013. https://doi.org/10.1039/C3CC44076A (2016).
21. Ceren, T. & Mehmet, C. Electronic structure, phonon and superconductivity for WP 5*d*-transition metal. *J. Appl. Phys.***126**, 175103. https://doi.org/10.1039/C3CC44076A (2019).
22. Autès, G., Gresch, D., Troyer, M., Soluyanov, A. A. & Yazyev, V. O. Robust type-II Weyl semimetal phase in transition metal diphosphides XP_2 (X = Mo, W). *Phys. Rev. Lett.***117**, 066402. https://doi.org/10.1039/C3CC44076A (2016).
23. Armitage, N. P., Mele, E. J., Vishwanath, A. & Vishwanath, A. Weyl and Dirac semimetals in three-dimensional solids. *Rev. Mod. Phys.***90**, 015001. https://doi.org/10.1021/cr00005a006 (2018).
24. Burkov, A. A., Hook, M. D. & Balents, L. Topological nodal semimetals. *Phys. Rev. B***84**, 235126. https://doi.org/10.1021/cr00005a006 (2011).
25. Volovik, G. E. Quantum phase transitions from topology in momentum space. In quantum analogues: from phase transitions to black holes and cosmology. *Phys. Scr.***164**, 31–73. https://doi.org/10.1021/cr00005a006 (2007).
26. Wang, J. T., Weng, H. & Chen, C. F. Topological nodal line semimetals in graphene network structures. *Adv Phys-X***4**, 1625724. https://doi.org/10.1021/cr00005a006 (2019).
27. Jin, H., Su, X. Y., Ni, N. & Zhi, M. Q. Transport of topological semimetals. *Annu. Rev. Mater. Res.***49**, 207–252. https://doi.org/10.1021/cr00005a006 (2019).
28. Heng, G., Jörn, V. . W. . F. ., Youngkuk, K. . & Andrew, R. . M. . Topological semimetals from first-principles. *Annu. Rev. Mater. Res.***49**, 153–183. https://doi.org/10.1021/cr00005a006 (2019).
29. Mondal, C., Barman, C. K., Kumar, S., Alam, A. & Pathak, B. Emergence of topological insulator and nodal line semi-metal states in XX'Bi (X= Na, K, Rb, Cs; X'= Ca, Sr). *Sci. Rep.***9**, 1–8. https://doi.org/10.1038/s41598-018-36869-0 (2019).
30. Huang, H., Liu, J., Vanderbilt, D. & Duan, W. Topological nodal-line semimetals in alkaline-earth stannides, germanides, and silicides. *Phys. Rev. B***93**, 201114. https://doi.org/10.1021/cr00005a006 (2016).
31. Wang, Z. *et al.* Dirac semimetal and topological phase transitions in A_3Bi (A= Na, K, Rb). *Phys. Rev. B***85**, 195320. https://doi.org/10.1021/cr00005a006 (2012).
32. Weng, H., Fang, C., Fang, Z., Bernevig, B. A. & Dai, X. Weyl semimetal phase in noncentrosymmetric transition-metal monophosphides. *Phys. Rev. X***5**, 011029. https://doi.org/10.1021/cr00005a006 (2015).
33. Wan, X., Turner, A. M., Vishwanath, A. & Savrasov, S. Y. Topological semimetal and Fermi-arc surface states in the electronic structure of pyrochlore iridates. *Phys. Rev. B***83**, 205101. https://doi.org/10.1021/cr00005a006 (2011).
34. Fang, C., Weng, H., Dai, X. & Fang, Z. Topological nodal line semimetals. *Chin. Phys. B***25**, 117106. https://doi.org/10.1002/celc.201600563 (2016).
35. Kim, Y., Wieder, B. J., Kane, C. L. & Rappe, A. M. Dirac line nodes in inversion-symmetric crystals. *Phys. Rev. Lett.***115**, 036806. https://doi.org/10.1002/celc.201600563 (2015).
36. Hyart, T., Ojajärvi, R. & Heikkilä, T. T. Two topologically distinct Dirac-line semimetal phases and topological phase transitions in rhombohedrally stacked honeycomb lattices. *J. Low Temp. Phys.***191**, 35–48. https://doi.org/10.1002/celc.201600563 (2018).
37. Liu, Z. K. *et al.* Discovery of a three-dimensional topological Dirac semimetal, Na_3Bi. *Science***343**, 864–867. https://doi.org/10.1002/celc.201600563 (2014).
38. Lv, B. *et al.* Observation of Fermi-arc spin texture in TaAs. *Phys. Rev. Lett.***115**, 217601. https://doi.org/10.1002/celc.201600563 (2015).
39. Hasan, M. Z. & Kane, C. L. Colloquium: Topological insulators. *Rev. Mod. Phys.***83**, 3045. https://doi.org/10.1002/celc.201600563 (2011).
40. Qi, X. L. & Zhang, S. C. Topological insulators and superconductors. *Rev. Mod. Phys.***83**, 1057. https://doi.org/10.1002/celc.201600563 (2011).
41. Xu, Q., Yu, R., Fang, Z., Dai, X. & Weng, H. Topological nodal lines semimetals in the CaP_3 family of materials. *Phys. Rev. B***95**, 045136. https://doi.org/10.1002/celc.201600563 (2017).
42. Chan, Y. H., Chiu, C. K., Chou, M. Y. & Schnyder, A. P. Ca_3P_2 and other topological semimetals with line nodes and drumhead surface states. *Phys. Rev. B***93**, 205132. https://doi.org/10.1002/celc.201600563 (2016).
43. Dong, X., Hu, M., He, J. L., Tian, Y. J. & Wang, H. T. A new phase from compression of carbon nanotube with anisotropic Dirac fermions. *Sci. Rep.***5**, 1–7. https://doi.org/10.1002/celc.201600563 (2015).
44. Feng, X. *et al.* Monoclinic C_{16}: sp^2-sp^3 hybridized nodal-line semimetal protected by *PT*-symmetry. *Carbon***127**, 527–532. https://doi.org/10.1016/j.ccr.2017.08.029 (2018).
45. Cheng, Y., Du, J., Melnik, R., Kawazoe, Y. & Wen, B. Novel three dimensional topological nodal line semimetallic carbon. *Carbon***98**, 468–473. https://doi.org/10.1016/j.ccr.2017.08.029 (2016).
46. Weng, H. *et al.* Topological node-line semimetal in three-dimensional graphene networks. *Phys. Rev. B***92**, 045108. https://doi.org/10.1016/j.ccr.2017.08.029 (2015).
47. Wang, J. T. *et al.* Body-centered orthorhombic C_{16}: A novel topological node-line semimetal. *Phys. Rev. Lett.***116**, 195501. https://doi.org/10.1016/j.ccr.2017.08.029 (2016).
48. Cheng, Y. *et al.* Body-centered tetragonal C_{16}: A novel topological node-line semimetallic carbon composed of Tetrarings. *Small***13**, 1602894–1602901. https://doi.org/10.1016/j.ccr.2017.08.029 (2017).

49. Chen, Y. *et al.* Nanostructured carbon allotropes with Weyl-like loops, points. *Nano Lett.***15**, 6974–6978. https://doi.org/10.1016/j.ccr.2017.08.029 (2015).
50. Li, Z. Z. *et al.* Orthorhombic carbon oC_{24}: A novel topological nodal line semimetal. *Carbon***133**, 39–43. https://doi.org/10.1016/j.ccr.2017.08.029 (2018).
51. Wang, J. T., Chen, C. F. & Kawazoe, Y. Topological nodal line semimetal in an orthorhombic graphene network structure. *Phys. Rev. B***97**, 245147. https://doi.org/10.1016/j.ccr.2017.08.029 (2018).
52. Wang, J. T., Qian, Y., Weng, H., Wang, E. G. & Chen, C. F. Three-dimensional crystalline modification of graphene in all-sp^2 hexagonal lattices with or without topological nodal lines. *J. Phys. Chem. Lett.***10**, 2515–2521. https://doi.org/10.1016/j.ccr.2017.08.029 (2019).
53. Wang, J. T., Nie, S., Weng, H. & Chen, C. F. Topological nodal-net semimetal in a graphene network structure. *Phys. Rev. Lett.***120**, 026402. https://doi.org/10.1016/j.ccr.2017.08.029 (2018).
54. Bu, K., Wang, J. T., Weng, H. & Chen, C. F. Topological semimetal in an sp^2-sp^3 hybridized carbon network with nodal rings. *Phys. Rev. B***101**, 205104. https://doi.org/10.1016/j.ijhydene.2015.02.099 (2020).
55. Jeitschko, W. & Donohue, P. C. The high pressure synthesis, crystal structure, and properties of CrP_4 and MoP_4. *Acta. Cryst.***28**, 1893–1898. https://doi.org/10.1016/j.ijhydene.2015.02.099 (1972).
56. Brown, A. Refinement of the crystal structure of black phosphorus. *Acta. Crystallogr.***19**, 684–685. https://doi.org/10.1016/j.ijhydene.2015.02.099 (1965).
57. Cheng, Y. *et al.* Sodium-induced reordering of atomic stacks in black phosphorus. *Chem. Mater.***29**, 1350–1356. https://doi.org/10.1016/j.ijhydene.2015.02.099 (2017).
58. Gong, N. *et al.* Structural diversity and electronic properties of 3d transition metal tetraphosphides, TMP_4 (TM= V, Cr, Mn, and Fe). *Inorg. Chem.***57**, 9385–9392. https://doi.org/10.1016/j.ijhydene.2015.02.099 (2018).
59. Winkler, B. *et al.* Crystal chemistry of molybdenum phosphides from density functional theory calculations. *J. Phys. Chem. Solids***64**, 405–411. https://doi.org/10.1016/j.ijhydene.2015.02.099 (2003).
60. Krukau, A. V., Vydrov, O. A., Izmaylov, A. F. & Scuseria, G. E. Influence of the exchange screening parameter on the performance of screened hybrid functionals. *J. Chem. Phys.***125**, 224106–224112. https://doi.org/10.1016/j.ijhydene.2015.02.099 (2006).
61. In our calculations, under standard GGA (without spin-orbital coupling) and TB model, MoP_4 also has a small nodal ring like as WP_4.
62. Marzari, N., Mostofi, A. A., Yates, J. R., Souza, I. & Vanderbilt, D. Maximally localized Wannier functions: theory and applications. *Rev. Mod. Phys.***84**, 1419. https://doi.org/10.1016/j.ijhydene.2015.02.099 (2012).
63. Mostofi, A. A. *et al.* A tool for obtaining maximally-localised Wannier functions. *Comput. Phys. Commun.***178**, 685–699. https://doi.org/10.1016/j.ijhydene.2015.02.099 (2008).
64. Po, H. C., Vishwanath, A. & Watanabe, H. Symmetry-based indicators of band topology in the 230 space groups. *Nat. Commun.***8**, 1–9. https://doi.org/10.1016/j.ijhydene.2015.02.099 (2017).
65. Song, Z., Zhang, T., Fang, Z. & Fang, C. Quantitative mappings between symmetry and topology in solids. *Nat. Commun.***9**, 1–7. https://doi.org/10.1021/cr400020d (2019).
66. Song, Z., Zhang, T. & Fang, C. Diagnosis for nonmagnetic topological semimetals in the absence of spin-orbital coupling. *Phys. Rev. X***8**, 031069. https://doi.org/10.1021/cr400020d (2018).
67. Jeitschko, W. & Rühl, R. Synthesis and crystal structure of diamagnetic ReP_4, a polyphosphide with Re-Re pairs. *Acta Crystallogr. B***35**, 1953–1958. https://doi.org/10.1021/cr400020d (1979).
68. Rühl, R., Jeitschko, W. & Schwochau, K. Preparation and crystal structures of technetium phosphides. *J. Solid State Chem.***44**, 134–140. https://doi.org/10.1021/cr400020d (1982).
69. Feng, S., Cheng, X., Cheng, X., Yue, J. & Li, J. Theoretical study on electronic, optical properties and hardness of technetium phosphides under high pressure. *Crystals.***7**, 176–185. https://doi.org/10.1021/cr400020d (2017).
70. Kresse, G. & Furthmüller, J. Efficient iterative schemes for ab initio total-energy calculations using a plane-wave basis set. *Phys. Rev. B***54**, 11169. https://doi.org/10.1021/cr400020d (1996).
71. Blöchl, P. E. Projector augmented-wave method. *Phys. Rev. B***50**, 17953. https://doi.org/10.1021/cr400020d (1994).
72. Perdew, J. P., Burke, K. & Ernzerhof, M. Generalized gradient approximation made simple. *Phys. Rev. Lett.***78**, 17954. https://doi.org/10.1021/cr400020d (1997).
73. Togo, A., Oba, F. & Tanaka, I. First-principles calculations of the ferroelastic transition between rutile-type and $CaCl_2$-type SiO_2 at high pressures. *Phys. Rev. B***78**, 134106. https://doi.org/10.1021/cr400020d (2008).
74. Mostofi, A. A. *et al.* An updated version of wannier90: A tool for obtaining maximally-localised Wannier functions. *Comp. Phys. Comm.***185**, 2309–2310. https://doi.org/10.1016/j.ijhydene.2015.02.099 (2014).
75. Wu, Q., Zhang, S., Song, H. F., Troyer, M. & Soluyanov, A. A. WannierTools: An open-source software package for novel topological materials. *Phys. Comm.***224**, 405–416. https://doi.org/10.1016/j.jcat.2006.05.014 (2018).
76. Momma, K. & Izumi, F. VESTA: a three-dimensional visualization system for electronic and structural analysis. *J. Appl. Cryst.***41**, 653–658. https://doi.org/10.1016/j.jcat.2006.05.014 (2008).

Acknowledgements

This study was supported by the National Natural Science Foundation of China (Grants No. 11974387 and No. 11674364) and the Strategic Priority Research Program of the Chinese Academy of Sciences (Grant No. XDB33000000).

Author contributions

M.R.K. and J.T.W. designed the study and wrote the paper; M.R.K and J.S.C. drawn Fig. 1, M.R.K. calculated the phonon band structures and plot Fig. 2, M.R.K. and K.B. calculated the electronic band structures and plot the Fig. 3, M.R.K. and J.S.C. plot the Fig. 4; all authors discussed the results and contributed to the manuscript.

Competing interests

The authors declare no competing interests.

Additional information

Supplementary information is available for this paper at https://doi.org/10.1038/s41598-020-68349-9.

Correspondence and requests for materials should be addressed to J.-T.W.

Reprints and permissions information is available at www.nature.com/reprints.